Journal of Colloid and Interface Science 582 (2021) 246–253

Contents lists available at ScienceDirect

Journal of Colloid and Interface Science

journal homepage: www.elsevier.com/locate/jcis

# Surface-modified nanoerythrosomes for potential optical imaging diagnostics

Marco Fornasier [a,b], Andrea Porcheddu [a], Anna Casu [c], Srinivasa R. Raghavan [d], Peter Jönsson [e], Karin Schillén [e], Sergio Murgia [a,b,*]

[a] Department of Chemical and Geological Sciences, University of Cagliari, s.s. 554 bivio Sestu, I-09042 Monserrato, Cagliari, Italy
[b] Translational Research Institute–AdventHealth, Orlando, FL, USA
[c] CSGI, Consorzio Interuniversitario per lo Sviluppo dei Sistemi a Grande Interfase, Via della Lastruccia 3, I-50019 Sesto Fiorentino, Florence, Italy
[d] Department of Chemical & Biomolecular Engineering, University of Maryland, College Park, MD 20742, USA
[e] Division of Physical Chemistry, Department of Chemistry, Lund University, P.O. Box 124, SE-22100 Lund, Sweden

## GRAPHICAL ABSTRACT

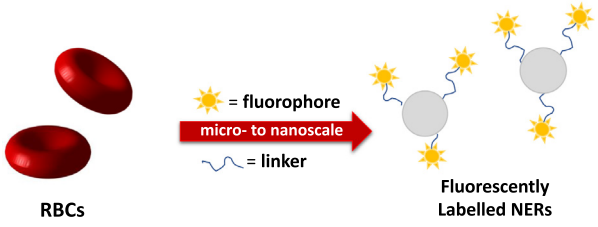


## ARTICLE INFO

*Article history:*
Received 26 April 2020
Revised 3 August 2020
Accepted 8 August 2020
Available online 14 August 2020

*Keywords:*
Cu-free click chemistry
Fluorescence
Red blood cells
Ghosts
Vesicles

## ABSTRACT

Nanoerythrosomes (NERs), vesicle-like nanoparticles derived from red blood cells, represent a new and interesting vector for therapeutic molecules and imaging probes, mainly thanks to their high stability and excellent biocompatibility. Aiming to present a proof-of-concept of the use of NERs as diagnostic tools for *in vitro*/*in vivo* imaging purposes, we report here several functionalization routes to decorate the surfaces of NERs derived from bovine blood with two different fluorophores: 7-amino-4-methylcumarin and dibenzocyclooctinecyanine5.5. Notably, the fluorophores were cross-linked to the NERs surface with glutaraldehyde and, in the case of dibenzocyclooctinecyanine5.5, also using a click-chemistry route, termed strain-promoted azide-alkyne cycloaddition. The physicochemical characterization highlighted the high stability of the NERs derivatives in physiological conditions. Furthermore, the loading efficiency of the fluorophores on the NERs surface was evaluated using both UV–Vis spectroscopy and fluorescence microscopy.



## 1. Introduction

The development of a robust therapeutic and diagnostic tools based on nanoparticles to manage diseases is a current goal in nanomedicine. These nanocarriers can significantly enhance the bioavailability of drugs and probes while minimizing the pharmacological side effects. Many carriers, such as cubosomes [1–5], hexosomes [6,7], silica nanoparticles [8,9], and vesicles [10–15], have been studied over the past years, and their efficacy via many administration routes has been proven.

Recent advances have opened the possibility of using cellular carriers such as erythrocytes, exosomes, leukocytes, and cancer cells [11,16–20]. These carriers meet several criteria desirable in clinical applications, such as biocompatibility and their unharmful

* Corresponding author at: Department of Chemical and Geological Sciences, University of Cagliari, s.s. 554 bivio Sestu, I-09042 Monserrato, Cagliari, Italy.
*E-mail addresses:* mfornasier@unica.it (M. Fornasier), murgias@unica.it (S. Murgia).

https://doi.org/10.1016/j.jcis.2020.08.032
0021-9797/

degradation products. Among the possible carriers, the so-called ghosts have gained attention as a valid alternative to other vectors. Ghosts can be obtained from red blood cells (RBCs) by removing the inner content (mostly hemoglobin) *via* hypotonic conditions. Unfortunately, due to their micrometric size, they exhibit fast *in vivo* clearance [11,21]. In 1994, Gaudreault and collaborators reported the first example of ghost nanoderivatives, named nanoerythrosomes (NERs) [22,23]. Being essentially vesicles (100 – 150 nm) derived by shearing (e.g., extrusion or sonication) of RBCs' ghosts, NERs do not show toxicity against different cell lines, and they are non-immunogenic in autologous administration [16,20,21,24,25]. The composition of the membrane gives NERs high versatility, both in the types of molecules that can be encapsulated and in the functionalization of their surface [21,26,27]. However, the high-shear process during NERs preparation can induce modification of the shell composition, especially removal of membrane proteins [26]. Interestingly, a recent work from Bóta et al. showed that addition of specific phospholipids originates a polygonal proteins scaffold that enhances the nanoerythrosomes stiffness and allows tailoring of these nanocarriers [28].

The coupling of targeting agents or imaging probes onto the surfaces of nanocarriers is a strategical step to minimize the leaching of these molecules (compared to merely encapsulating the molecules in the lumen of the nanocarriers). In this regard, *Click Chemistry* has proven to be a powerful tool in chemistry for gaining insight into biology, and nanomedicine. Exploiting a reaction among an azide and an alkyne catalyzed by copper (Cu, copper-catalyzed azide alkyne cycloaddition, CuAAC) species, it is possible to obtain a stable covalent 1,2,3-triazole ring conjugate. Such azide-alkyne cycloaddition has found a wide variety of practical applications across many different scientific sectors, especially in cell membrane functionalization [29–31]. The presence of Cu catalysts could affect the cell microenvironment, and a Cu-free click-chemistry route called "*strain-promoted azide-alkyne cycloaddition*" (SpAAC) represents a superior alternative. In this latter case, the reaction is promoted by a strain on the alkyne or azide, without any Cu catalysts. The benefits of SpAAC include biocompatibility, stability, specificity, and bio-orthogonality [4,30,32,33]. The SpAAC is preferable whenever a small concentration of Cu can affect protein folding or cell function [33,34].

Fluorescence light has been widely used in medical imaging [35–37]. The proper choice of a fluorescent probe is crucial, since UV–Vis and near-infrared (NIR) emitters can be adopted for imaging applications *in vitro* and *in vivo*, respectively. In the latter case, features such as minimal autofluorescence and adsorption in tissue are advantages of the so-called "NIR window", within the range 650–900 nm. Consequently, fluorophores emitting in the NIR region are a valuable asset for *in vivo* diagnostics [3,38]. Moreover, compared with visible light, NIR fluorescence wavelengths allow high-sensitivity real-time image guidance in different surgery protocols [35–37,39].

So far, the application of NERs as probes for optical imaging has barely been studied [24,40,41]. Therefore we explored the possibility of using this kind of nanovectors as imaging tools for *in vitro*/*in vivo* applications by labelling their surface with two fluorescent dyes (a coumarin and a cyanine derivative). Specifically, labelling was realized by using the cross-linking method with glutaraldehyde, and the first example of SpAAC Click Chemistry applied to NERs.

## 2. Material and methods

### 2.1. Materials

Bovine blood was obtained from Istituto Zooprofilattico della Sardegna and withdrawn from a healthy two-years-old cow, during a routine clinical examination. Na-EDTA (1.5 mg per mL of blood) was added to blood samples to avoid coagulation of RBCs, thereafter the samples were stored at 4 °C before any manipulation. The blood was used no longer than 2 h after withdrawal.

Glutaraldehyde 50% v/v, 7-amino-4-methylcoumarin (AMC), 3-azido-1-propylamine were purchased from TCI Chemicals (Belgium). Sodium chloride, sodium phosphate dibasic, potassium chloride and sodium phosphate monobasic were purchased from Sigma Aldrich S.r.L. (Italy). The fluorophore dibenzocyclooctinecyanine5.5 (DBCO-Cy5.5) was purchased from Lumiprobe GmbH (Germany).

Fresh distilled water was purified using a Milli-Q system (Millipore Corporation, Bedford, MA, U.S.) for standards preparation, and it was filtered with a 0.22 μm pore size hydrophilic Millipore filter before any use.

### 2.2. Preparation of NERs

The protocol used in this work for the preparation of Nanoerythrosomes was derived from the one proposed by Raghavan and collaborators [25]. It can be divided into four steps (three centrifugation steps and one ultrasonication process) described as following. The first step is the extraction of the red blood cells: blood (usually 80 mL and divided in four fractions of 20 mL each) was diluted with 30 mL of cold phosphate-buffered saline (PBS) solution at pH 7.4 and centrifuged at 1859 g at 4 °C for 15 min. The light-yellow supernatant (mainly plasma) was removed, the red pellet at the bottom of the tube (RBCs) was washed with 30 mL of cold PBS solution at pH 7.4 and then dispersed. This step was repeated until the supernatant appeared colorless and transparent, usually three times. In the second step, the RBCs were lysed in a hypotonic environment. After the removal of the supernatant, they were dispersed in 30 mL of cold hypotonic solution 0.5% wt of NaCl and incubated for 30 min in a cold bath. The dark red solution (derived from the release of hemoglobin) was then centrifuged at 10,706*g* for 15 min at 4 °C. The supernatant was removed, and the pellet was resuspended and washed with cold PBS solution at pH 7.4 and dispersed in the medium. This step was repeated until the pellet appeared cream-colored or light yellow (usually three times), to remove most of hemoglobin from RBCs. In the third step, microerythrosomes (MERs) were formed: the pellet obtained in the previous step was dispersed in 30 mL of cold PBS solution at pH 7.4 and centrifuged at 24,088*g* for 15 min at 4 °C. The supernatant was removed, the pellet was resuspended in PBS and dispersed again. This step was repeated three times. Finally, in the fourth and final step, nanoerythrosomes were formed. The cream-color pellet was resuspended in 3 mL of PBS 10 mM at pH 7.4 and sonicated for 5 min using a tip-sonicator and the temperature of the dispersion was controlled using a water bath. The pulse of the sonicator was set to 90% of amplitude, having 1 s of sonication (ON) and 1 s of break (OFF). The solution was then filtered three times through a 2.7 μm pore size membrane from Millipore. After an additional 10 min of sonication with the same set-up as before, a bluish and homogeneous colloidal dispersion of NERs was obtained.

### 2.3. Functionalization of NERs surface by cross-linking

The first surface functionalization to fluorescently label the NERs is based on a cross-linking method using glutaraldehyde [23]. 100 μL of 0.5% v/v solution of glutaraldehyde was added to 1 mL of NERs formulation in 1 mL of PBS at pH 7.4. Then 1 mg of the fluorescent dye AMC was added to the solution under mild stirring at room temperature in the dark for 1 h. A solution of glycine 15% v/v in PBS at pH 7.4 was added to stop the reaction and the formulation was stored at 25 °C overnight. The day after, the formulation appeared as a light yellow solution, and it was purified from

the free fluorophore by dialysis, loading 2 mL of formulation into a dialysis tubing cellulose membrane (14 kDa molecular weight cut-off, purchased from Sigma Aldrich) and dialyzing it against 2 L of PBS pH 7.4 for 2 h by replacing the buffer after 1 h at room temperature in the dark. The formulation NER-F1 was thereafter stored at 25 °C until use.

### 2.4. Functionalization of NERs surface with cross-linking and SpAAC method

By implementing Click Chemistry into the previous functionalization, we were able to obtain the formulation NER-F2 as follows. 100 μL of 0.5% v/v solution in PBS of glutaraldehyde 5 μL of 3-azido-1-propylamina were added to 1 mL of NERs formulation in another 1 mL of PBS at pH 7.4. It was let under mild stirring for 1 h in the dark at room temperature. The bright pink solution was dialyzed to remove the free 3-azido-1-propylamina, following the procedure described in the previous section. Then, 1 mg of DBCO-Cy5.5 was added to the formulation and it was let under mild stirring overnight at room temperature in the dark. The formulation appeared as a light purple/blue solution with some dark blue precipitate (the fluorophore) at the bottom of the tube. 2 mL of the formulation was loaded into a dialysis tubing cellulose membrane (14 kDa MW cutoff, purchased from Sigma Aldrich) and dialyzed again 2 L of PBS pH 7.4 for 2 h (by replacing the buffer after 1 h) at room temperature in the dark. NER-F2 was stored at 25 °C.

### 2.5. Dynamic light scattering and electrophoretic light scattering

The three samples, NERs, NER-F1 and NER-F2 were diluted 1:50 with PBS pH 7.4 solution prior to any measurement and were analyzed within 24 h after preparation. Their hydrodynamic size was measured by Dynamic Light Scattering using a ZetaSizer Nano ZS instrument (Malvern Instruments/Malvern Panalytical), Malvern, U.K.) at a temperature of 25.0 ± 0.1 °C [42]. The instrument is equipped with a 4 mW He–Ne laser (operating at a wavelength of 633 nm) and the light scattering measurements were performed in a backscattering geometry at a scattering angle of 173°. The same instrument was used for the determination of the ζ-potential (using the Smoluchowski's equation) from measurements of the electrophoretic mobility in DTS1070 disposable folded capillary cells at the scattering angle of 13°. The intensity-weighted hydrodynamic diameter ($D_h$) and the polydispersity index (PdI) extracted from a second-order Cumulant analysis as well as the ζ-potential are reported as averages of six consecutive measurements.

### 2.6. Effect of sonication on NERs size

We studied how the sonication time affects NER's size. After each sonication cycle (5, 6, 8, 10, 15, 20 and 30 min), a portion of the dispersion was diluted with the buffer (1:50) and then the hydrodynamic diameter was determined using DLS.

### 2.7. Cryogenic transmission electron microscopy

The morphology of the NERs was examined using a JEM-2200FS transmission electron microscope (JEOL) specially optimized for cryo-TEM at the National Center for High Resolution Electron Microscopy (nCHREM) at Lund University. It is equipped with a field-emission electron source and an in-column energy filter (omega filter). The images were recorded under low-dose conditions with 15 eV slit width in place, adopting an acceleration voltage of 200 kV on a bottom-mounted TemCam-F416 camera (TVIPS) using SerialEM. Each sample was prepared using an automatic plunge freezer system (Leica Em GP) with the environmental chamber operated at 21.0 °C and 90% of relative humidity. A droplet (4 μL) of the NERs formulation was deposited on a lacey formvar carbon-coated grid (Ted Pella) and was blotted with filter paper to remove excess fluid. The grid was then plunged into liquid ethane (around −183 °C) to ensure the rapid vitrification of the sample in its native state. Prior to the Cryo-TEM measurements, the specimens were stored in liquid nitrogen (−196 °C) before imaging microscope using a cryo-transfer tomography holder (Fischione Model 2550).

### 2.8. Photophysical measurements

NER-F1 and NER-F2 were studied through ultraviolet–visible (UV–Vis) absorption and steady-state fluorescence spectroscopy using a Win-CaryVarian UV–Vis double-beam spectrophotometer and a Win-CaryVarian Fluorimeter respectively, after dilution 1:10 and 1:500. The absorption spectra of the two fluorophores were measured in 1 cm quartz cuvettes from which the background was subtracted by using the pure solvent. The fluorescence signal was measured using 5.0 and 2.5 slits aperture, for excitation and emission respectively. AMC was excited at 351 nm and DBCO-Cy5.5 at 680 nm. The dyes loading was measured three times using the calibration curve methods in the UV–Vis range:

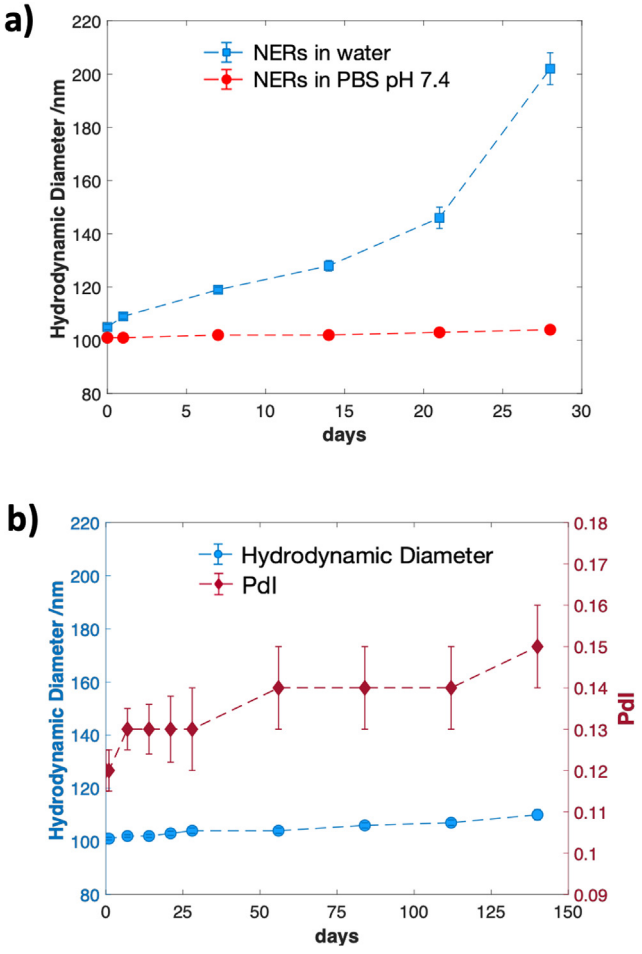


**Fig. 1.** (a) The apparent hydrodynamic diameter ($D_h$) of the NER particles in water as a function of time after preparation. (b) Stability of the NERs in PBS pH 7.4 in terms of $D_h$ and polydispersity index (PdI) of the formulation over 5 months. The dashed lines are guides for the eyes. Both $D_h$ and PdI were obtained from a second-order Cumulant analysis of the measured intensity-intensity autocorrelation functions.

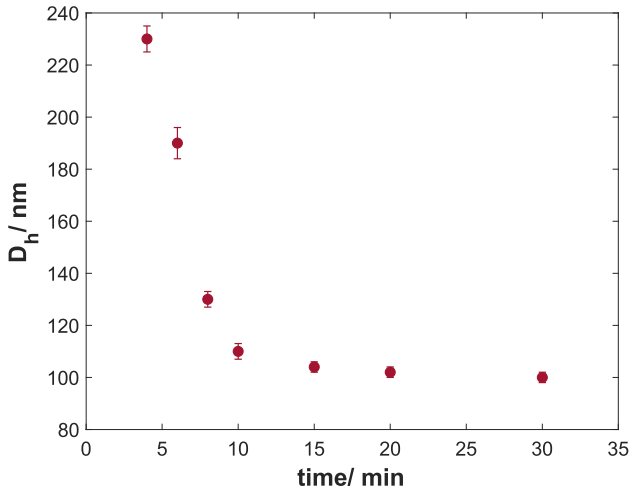


**Fig. 2.** Evaluation of sonication time on the apparent hydrodynamic diameter ($D_h$) of the NERs.

the measurements were performed in MeOH/$H_2O$: 3/1 buffered at pH 7.4 for the free AMC and NER-F1. Since the solubility of DBCO-Cy5.5 in DMSO, the analyses for NER-F2 were performed in a DMSO/$H_2O$: 3/1 mixture buffered at pH 7.4. The free dyes excitation and emission spectra were acquired in MeOH and DMSO (data not shown).

### *2.9. Fluorescence single molecule microscopy*

The DBCO-Cy5.5-labelled NERs were studied with a Nikon Apo TIRF 100× magnification oil immersion objective on a customized Nikon Eclipse Ti Eclipse microscope equipped with a Photometrics Prime 95B scientific CMOS. The DBCO-Cy5.5-labelled NERs were diluted 1:100 in PBS and added to a cover glass slide (25 mm diameter, No 1, VWR), resulting in approximately 500 NERs in the image field of view. The sample was illuminated using an Oxxius diode laser operating at a wavelength of 638 nm (180 mW). The acquired images were 600 pixels by 600 pixels with a pixel size of 0.11 μm by 0.11 μm and were acquired at an exposure time of 100 ms. The individual NER-F2 particles were detected using the MATLAB script pkfnd.m (http://site.physics.georgetown.edu/matlab/code.html) after background subtraction. Photobleaching steps were obtained by continuously taking images until the particles bleached.

## 3. Results and discussion

The RBC vesicles were obtained from a total bovine blood sample according to a procedure that slightly alters that reported by Raghavan et al. [25]. It consisted of several centrifugation and washing steps to purify the RBCs. The centrifugation steps are required first to separate the blood cells from plasma. Then, by tuning the concentration of the hypotonic solution from 0.85% w/v to 0.5% w/v, the membranes of the RBCs were osmolyzed to ensure the complete release of the hemoglobin content. The membrane materials are finally resealed in an isotonic environment (PBS buffer 10 mM at pH 7.4) and ultrasonicated to obtain the nanoderivatives, i.e. the NERs. Initially, large aggregates (ca. 3–4 μm) were observed by DLS, even after 20 min of sonication (data not shown). Therefore, an extrusion method was implemented in the preparation of the nanoparticles, in order to remove larger aggregates. After extrusion through a filter (2.7 μm pore size), the dispersion was ultrasonicated again to reduce the size to ca. 100 nm. The appearance of the dispersion after the final sonication step was transparent and bluish.

As it is possible to obtain NERs both in water and buffers, we evaluated their stability over one month in terms of their hydrodynamic diameter ($D_h$) in each media using DLS. As reported in Fig. 1a, the apparent hydrodynamic diameter in water and physiological buffer at 25 °C is initially ca. 100 nm, while the ζ-potentials –18 mV and –30 mV were respectively recorded for NERs dispersed in water or PBS buffer.

By aging, the sample in water exhibited an increasing trend in terms of size and polydispersity. On the contrary, the size and polydispersity of NERs in 1x PBS pH 7.4 (10 mM) remained stable without any significant changes over one month (between measurements, the NERs were stored at 25 °C), most likely because of the higher negative surface charge of NERs in PBS buffer that better prevents flocculation of the nanoparticles. For this reason, PBS was used as a buffer to investigate further NERs morphology, stability, and physicochemical features.

First, the long-time stability of the NER particles in this formulation was followed in terms of $D_h$ over five months (Fig. 1b). As reported above, the sample was stored at 25 °C

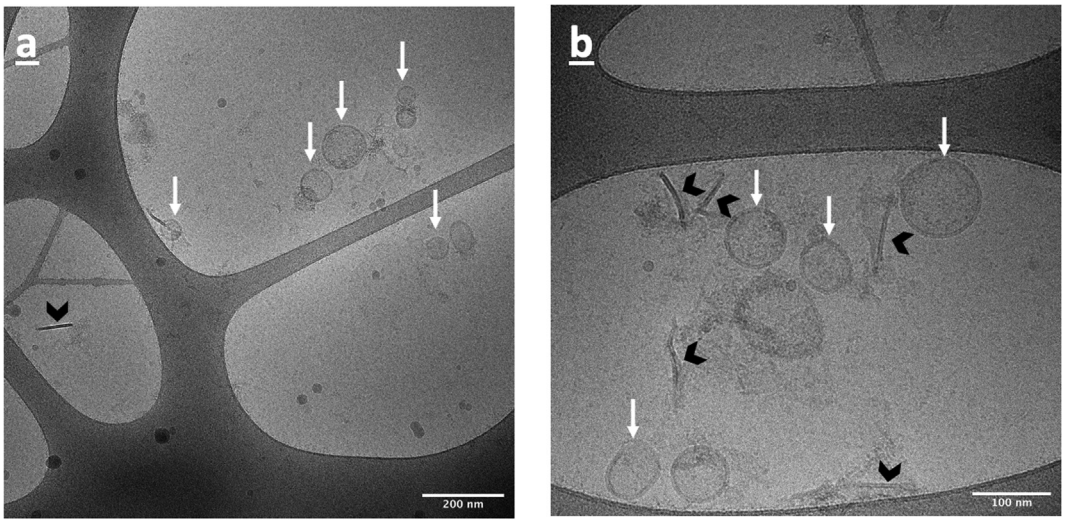


**Fig. 3.** NERs cryo-TEM image in PBS buffer at pH 7.4 10 mM at two different magnitudes (a at ×40k and b at ×80k). Several membranes not reassembled into vesicles are indicated by black arrowheads. The white arrows point toward spherical unilamellar vesicles.

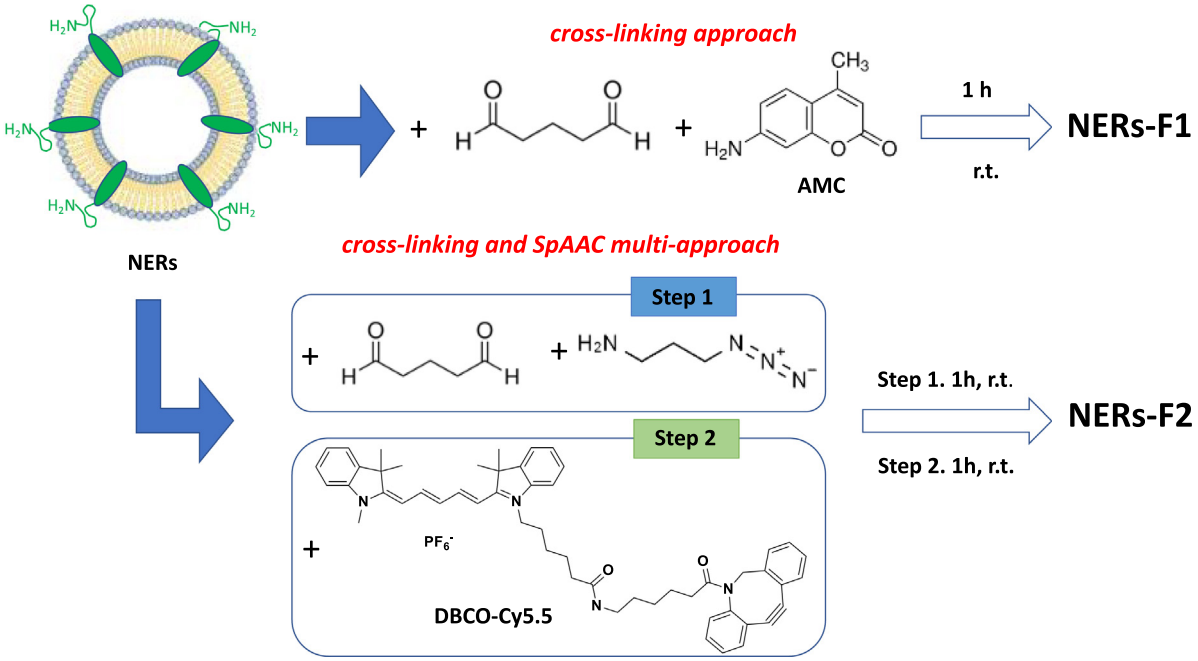


**Scheme 1.** Surface modification to obtain NERs-F1 and NERs-F2.

**Table 1**
Hydrodynamic diameters ($D_h$), polydispersity index (PdI) and ζ-potentials of the unlabeled and labelled formulations.

| Formulation | $D_h$ [nm] | PdI | ζ-potential [mV] |
|---|---|---|---|
| NERs | 101 ± 1 | 0.12 ± 0.01 | −31.2 ± 1.1 |
| NERs-F1 | 120 ± 4 | 0.20 ± 0.01 | −23.2 ± 2.1 |
| NERs-F2 | 127 ± 4 | 0.18 ± 0.02 | −24.0 ± 2.3 |

between each measurement. As noticed, the hydrodynamic diameter and the accompanied polydispersity index remained almost constant during the investigated temporal range, hence indicating that aging did not affect the dispersion significantly in terms of size. It is worth noticing that the polydispersity indices measured for the formulations here investigated are in good agreement with those reported in literature in similar systems [25,40].

The size of the vesicles strongly depends on the sonication conditions adopted during the sample preparation. Therefore, the effect of sonication time on the size was investigated sonicating the sample for 5, 6, 8, 10, 15, 20, and 30 min after the extrusion procedure.

As shown in Fig. 2, after 5 min, the NER particles showed a quite large size. While increasing the sonication time, their size decreased, reaching a plateau at 10 min. These features were not reduced further by longer sonication times, probably because the cytoskeleton material constituting the NERs membrane does not allow a further reduction of the bilayer curvature.

Cryo-TEM images reported in Fig. 3a and b showed that the NERs exhibit in 1x PBS at pH 7.4 mostly unilamellar vesicles with spherical shape (white arrows) coexisting with some membranes not reassembled into vesicles (black arrowheads). Although no direct evidence can be obtained from this formulation, it was already reported that the morphology of these nanoparticles in

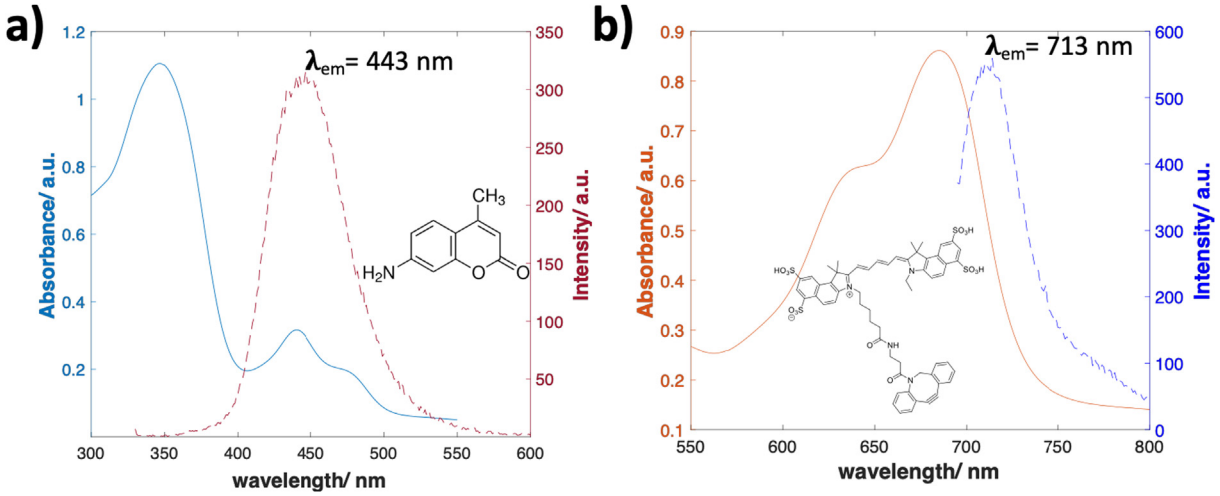


**Fig. 4.** Absorption and emission spectra for NERs-F1 (a) and NERs-F2 (b) after dilution 1:500 in PBS pH 7.4 medium.

hypertonic conditions is reminiscent of that exhibited by RBCs, showing the same biconcave structure [25]. This finding suggests that, after the hypotonic lysis, the membrane may reassemble in its native conformation. However, a membrane flipping during the reconstituting process cannot be fully excluded. In addition, the sonication process could solubilize some membrane proteins that aggregates in solution with their lipid surroundings [26], originating part of the particulate material observed in Fig. 3a and b.

The retention of membrane structures, e.g. proteins, lipids, and glycolipids, on NERs surface and the possible use of their —$NH_2$ terminal groups for a functionalization process was already hypothesized and exploited by Lejeune, who applied the cross-linking method to decorate the NERs surface with daunorubicin [23]. Accordingly, glutaraldehyde was here used as a cross-linker to have a first layer on which the fluorophores (i) AMC and (ii) DBCO-Cy5.5 were attached using SpAAC Click Chemistry to obtain NERs-F1 and NERs-F2, respectively (Scheme 1).

The reactions required dark conditions to avoid glutaraldehyde polymerization. These labelled NER particles had an apparent $D_h$ around 120 nm and were characterized by a slightly larger PdI with respect to bare NERs (see Table 1).

Moreover, a decrease of the ζ-potential values for both NERs-F1 and NERs-F2 was recorded compared to unlabeled NERs, a finding certainly related to the functionalization of the membrane proteins that removes charged groups in the electric double layer.

AMC is a commercial dye that absorbs at 350 nm and emits at 430 nm in MeOH, whereas the DBCO-Cy5.5 fluorophore absorbs the radiation in the red (680 nm) and has a fluorescence emission around 710 nm in DMSO. The maxima of absorption in the UV–Vis region for both dyes, 350 nm for AMC and 680 nm for DBCO-Cy5.5, respectively (Fig. 4a and b), were used to quantify the fluorophores covalently linked to the surface of NERs using the curve calibration method.

The concentration of the dyes was found to be $(5.2 \pm 0.8) \times 10^{-5}$ M in the case of AMC and $(9.2 \pm 0.7) \times 10^{-6}$ M in the case of DBCO-Cy5.5. It is important to address that small membrane fragments or proteins/lipids aggregates could be solubilized during the sonication step. This material in solution can affect the functionalization ratio.

The absorption spectra and the emission fluorescence spectra for the NERs-F1 and NERs-F2 are reported in Fig. 4, where AMC and DBCO-Cy5.5 exhibit an emission band with a maximum at 443 nm and 713 nm, respectively. The small red shift observed for both dyes in comparison with the free dye emission indicates they are experiencing a more polar environment. Also, NERs-F1 and NERs-F2 showed a strong fluorescence emission signal after dilution up to 1:500 in PBS medium. These two fluorescent formulations can be recognized as suitable candidates for optical imaging *in vitro* (NERs-F1) and *in vivo* (NERs-F2).

Since we have already stressed the importance of having an *in vivo* tool for optical imaging, the NERs-F2 formulation was furthermore analyzed using single-molecule fluorescence microscopy at an excitation wavelength of 638 nm (Fig. 5a). Individual NERs-F2 particles could be discerned in the microscopy images and the intensity from two separate measurements gave the fluorescence intensity distribution shown in Fig. 5b.

A typical fluorescence intensity was about 30 counts (Fig. 5b), whereas the average intensity from all 1100 detected NERs-F2 particles was 80 counts. The 30 counts correspond approximately to the fluorescence from one DBCO-Cy5.5 fluorophore, which could be estimated from the abrupt change in intensity when one of the NERs-F2 particles exhibited bleaching (Fig. 5c). This means that the average number of dye molecules is roughly 2.5 per labelled NE2-F2 particle. However, most of the labelled NERs-F2 contains only one fluorophore. This data corresponded to the very low amount of DBCO-Cy5.5 used for the preparation of NERs-F2.

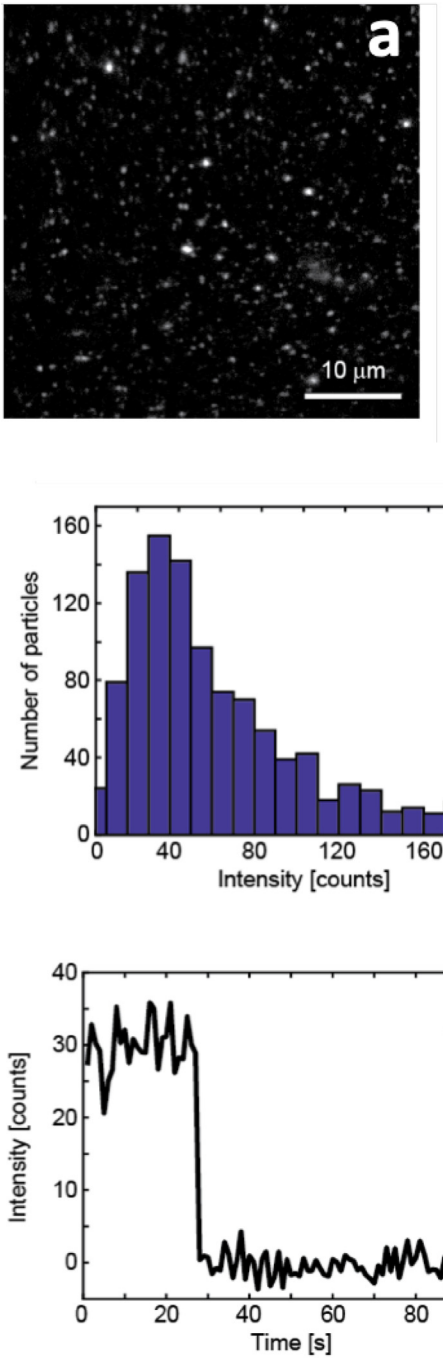


**Fig. 5.** Single-molecule fluorescence imaging of NERs-F2. (a) A representative fluorescence image showing NER-F2 particles absorbed to a glass slide. (b) Histogram of the intensity distribution from individually detected NERs-F2. The data is from two measurements with a total of 1124 detected particles. Approximately 7% of the particles have an intensity larger than 200 counts. (c) The change in intensity when bleaching a representative NER-F2 particle in (a).

Indeed, by increasing the concentration, it would be possible to obtain a higher number of dye molecules per nanoparticle, increasing the fluorescence signal consequently.

## 4. Conclusions

Given the high demand for finding novel, biocompatible, biodegradable, and non-cytotoxic tools in nanomedicine, the physicochemical properties of unlabeled, and fluorescently labelled nanoerythrosomes (nanoderivatives of bovine red blood

cells) were here investigated. Indeed, NERs are a new class of drug and imaging probe carriers engineered to reduce the biological impact at a minimum, with excellent perspectives in personalized medicine.

NERs applicability in the imaging field has not been established yet. Therefore, different functionalization methods to achieve fluorescent labelling of this kind of nanoparticles were presented in this work. The first case of Click Chemistry on NERs was reported, showing how SpAAC could come in aid to functionalize such kind of nanocarriers. NERs stability was investigated in two different media and over time, highlighting that the physiological PBS was the best buffer to prepare and store the nanoparticles. Given their high colloidal stability and physico-chemical features, NERs represent an interesting alternative to other drug carriers, especially when biocompatibility is an issue. Indeed, they could be harvested directly from a patient blood, thus the immunological response should be negligible. Two different fluorophores were successfully conjugated on NERs surface for imaging applications: AMC and DBCO-Cy5.5. The spectroscopic properties of the labelled formulations showed that in both cases the dyes are experiencing a polar environment, being oriented towards the bulk water. Remarkably, the loading efficiency on NERs surfaces and their fluorescence properties after high dilution ratio (1:500) suggest that fluorescently labelled nanoerythrosomes can be used as a potent imaging tool *in vitro* and *in vivo*.

Drugs can be either encapsulated within the NERs core [43] or conjugated on their surface [23]. Particularly, by combining the versatility of different functionalization routes, e.g. Click Chemistry and cross-linking, with NERs intrinsic biocompatibility, these surface-modified systems could assist in several clinical therapies and imaging applications. However, given the desired application in nanomedicine, these nanovectors should be tested against different cell lines to understand possible difference in terms of uptake in comparison with other soft matter-based formulations. Different groups can be used to conjugate therapeutic molecules or imaging probes to the NERs surface (such as —COOH, —OH, —SH and, of course $NH_2$) [16], and new decoration routes of NERs surface could represent another possible outlook, possibly with targeting agents to achieve selective delivery of therapeutic agents. Nevertheless, surface functionalization should be evaluated with care to avoid activation of the complement with consequent reduction of the NERs permanence in the bloodstream because of RES clearance [44].

## CRediT authorship contribution statement

**Marco Fornasier:** Investigation, Writing - review & editing. **Andrea Porcheddu:** Investigation, Writing - review & editing. **Anna Casu:** Data curation, Writing - review & editing. **Srinivasa R. Raghavan:** Supervision, Writing - review & editing. **Peter Jönsson:** Investigation, Writing - review & editing. **Karin Schillén:** Supervision, Writing - review & editing. **Sergio Murgia:** Supervision, Funding acquisition, Writing - original draft.

## Declaration of Competing Interest

The authors declare that they have no known competing financial interests or personal relationships that could have appeared to influence the work reported in this paper.

## Acknowledgements

The authors thank Dr. Manuel Liciardi and Dr. Giuseppe Argiolas from Istituto Zooprofilattico della Sardegna, who kindly provided the bovine blood samples. They also thank the National Center for High Resolution Electron Microscopy (nCHREM) at Lund University is kindly thanked for providing access to the executing the Cryo-TEM measurements, and Dr. Anna M. Carnerup for her assistance and advices for these measurements. M.F. Ph.D. scholarship was funded by the project P.O.R. Sardegna F.S.E. 2014–2020. S.M. thanks Fondazione Banco di Sardegna and Regione Autonoma della Sardegna (Progetti Biennali di Ateneo Annualità 2018)

## References

[1] H.M.G. Barriga, M.N. Holme, M.M. Stevens, Cubosomes: The next generation of smart lipid nanoparticles?, Angew Chemie – Int. Ed. 58 (2019) 2958–2978, https://doi.org/10.1002/anie.201804067.
[2] U. Bazylińska, J. Kulbacka, J. Schmidt, Y. Talmon, S. Murgia, Polymer-free cubosomes for simultaneous bioimaging and photodynamic action of photosensitizers in melanoma skin cancer cells, J. Colloid Interface Sci. 522 (2018) 163–173, https://doi.org/10.1016/j.jcis.2018.03.063.
[3] S. Biffi, L. Andolfi, C. Caltagirone, C. Garrovo, A.M. Falchi, V. Lippolis, A. Lorenzon, P. Macor, V. Meli, M. Monduzzi, M. Obiols-Rabasa, L. Petrizza, L. Prodi, A. Rosa, J. Schmidt, Y. Talmon, S. Murgia, Cubosomes for in vivo fluorescence lifetime imaging, Nanotechnology 28 (2017), https://doi.org/10.1088/1361-6528/28/5/055102.
[4] N. Alcaraz, Q. Liu, E. Hanssen, A. Johnston, B.J. Boyd, Clickable cubosomes for antibody-free drug targeting and imaging applications, Bioconjugate Chem. 29 (2018) 149–157, https://doi.org/10.1021/acs.bioconjchem.7b00659.
[5] L. Boge, K. Hallstensson, L. Ringstad, J. Johansson, T. Andersson, M. Davoudi, P.T. Larsson, M. Mahlapuu, J. Håkansson, M. Andersson, Cubosomes for topical delivery of the antimicrobial peptide LL-37, Eur. J. Pharm. Biopharm. 134 (2019) 60–67, https://doi.org/10.1016/j.ejpb.2018.11.009.
[6] M.M. Ebersold, M. Petrović, W.K. Fong, D. Bonvin, H. Hofmann, I. Milošević, Hexosomes with undecylenic acid efficient against candida albicans, Nanomaterials 8 (2018), https://doi.org/10.3390/nano8020091.
[7] L. Rodrigues, K.N. Raftopoulos, S. Tandrup Schmidt, F. Schneider, H. Dietz, T. Rades, H. Franzyk, A.E. Pedersen, C.M. Papadakis, D. Christensen, G. Winter, C. Foged, M. Hubert, Immune responses induced by nano-self-assembled lipid adjuvants based on a monomycoloyl glycerol analogue after vaccination with the Chlamydia trachomatis major outer membrane protein, J. Control. Release. 285 (2018) 12–22, https://doi.org/10.1016/j.jconrel.2018.06.028.
[8] N. Iturrioz-Rodríguez, M.A. Correa-Duarte, M.L. Fanarraga, Controlled drug delivery systems for cancer based on mesoporous silica nanoparticles, Int. J. Nanomed. 14 (2019) 3389–3401, https://doi.org/10.2147/IJN.S198848.
[9] V. López, M.R. Villegas, V. Rodríguez, G. Villaverde, D. Lozano, A. Baeza, M. Vallet-Regí, Janus mesoporous silica nanoparticles for dual targeting of tumor cells and mitochondria, ACS Appl. Mater. Interfaces 9 (2017) 26697–26706, https://doi.org/10.1021/acsami.7b06906.
[10] M. Schlich, M. Fornasier, M. Nieddu, C. Sinico, S. Murgia, A. Rescigno, 3-hydroxycoumarin loaded vesicles for recombinant human tyrosinase inhibition in topical applications, Colloids Surf. B Biointerfaces 171 (2018) 675–681, https://doi.org/10.1016/j.colsurfb.2018.08.008.
[11] S. Valkonen, E. van der Pol, A. Böing, Y. Yuana, M. Yliperttula, R. Nieuwland, S. Laitinen, P.R.M. Siljander, Biological reference materials for extracellular vesicle studies, Eur. J. Pharm. Sci. 98 (2017) 4–16, https://doi.org/10.1016/j.ejps.2016.09.008.
[12] M. Schlich, C. Sinico, D. Valenti, A. Gulati, M.D. Joshi, V. Meli, S. Murgia, T. Xanthos, Towards long-acting adrenaline for cardiopulmonary resuscitation: Production and characterization of a liposomal formulation, Int. J. Pharm. 557 (2019) 105–111, https://doi.org/10.1016/j.ijpharm.2018.12.044.
[13] M. Mamusa, L. Sitia, F. Barbero, A. Ruyra, T.D. Calvo, C. Montis, A. Gonzalez-Paredes, G.N. Wheeler, C.J. Morris, M. McArthur, D. Berti, Cationic liposomal vectors incorporating a bolaamphiphile for oligonucleotide antimicrobials, Biochim. Biophys. Acta – Biomembr. 2017 (1859) 1767–1777, https://doi.org/10.1016/j.bbamem.2017.06.006.
[14] M. Mamusa, F. Barbero, C. Montis, L. Cutillo, A. Gonzalez-Paredes, D. Berti, Inclusion of oligonucleotide antimicrobials in biocompatible cationic liposomes: A structural study, J. Colloid Interface Sci. 508 (2017) 476–487, https://doi.org/10.1016/j.jcis.2017.08.080.
[15] M. Schlich, F. Longhena, G. Faustini, C.M. O'Driscoll, C. Sinico, A.M. Fadda, A. Bellucci, F. Lai, Anionic liposomes for small interfering ribonucleic acid (siRNA) delivery to primary neuronal cells: Evaluation of alpha-synuclein knockdown efficacy, Nano Res. 10 (2017) 3496–3508, https://doi.org/10.1007/s12274-017-1561-z.
[16] H. Zhang, Erythrocytes in nanomedicine: an optimal blend of natural and synthetic materials, Biomater. Sci. 4 (7) (2016) 1024–1031, https://doi.org/10.1039/c6bm00072j.
[17] C. Gutiérrez Millán, D.G. Bravo, J.M. Lanao, New erythrocyte-related delivery systems for biomedical applications, J. Drug Deliv. Sci. Technol. 42 (2017) 38–48, https://doi.org/10.1016/j.jddst.2017.03.019.
[18] N. Kavita, P. Sayali, S.A. Payghan, Design of three-factor response surface optimization of camouflaged capecitabine nanoerythrovesicles, Asian J. Pharm. 10 (2016) 306–321.
[19] V. Balasubramanian, A. Poillucci, A. Correia, H. Zhang, C. Celia, H.A. Santos, Cell membrane-based nanoreactor to mimic the bio-compartmentalization

strategy of a cell, ACS Biomater. Sci. Eng. 4 (2018) 1471–1478, https://doi.org/10.1021/acsbiomaterials.7b00944.
[20] R. Hirlekar, P. Patel, N. Dand, V. Kadam, Drug loaded erythrocytes: as novel drug delivery system, Curr. Pharm. Des. 14 (2008) 63–70, https://doi.org/10.2174/138161208783330772.
[21] K.A. Nangare, S.D. Powar, S.A. Payghan, Nanoerythrosomes: Engineered 2016 (2016) 223–233.
[22] J. Désilets, A. Lejeune, J. Mercer, C. Gicquaud, Nanoerythrosomes, a new derivative of erythrocyte ghost: IV. Fate of reinjected nanoerythrosomes, Anticancer Res. (2001).
[23] A. Lejeune, M. Moorjani, C. Gicquaud, J. Lacroix, P. Poyet, C.R. Gaudreault, Nanoerythrosome, a new derivative of erythrocyte ghost: Preparation and antineoplastic potential as drug carrier for daunorubicin, Anticancer Res. 14 (1994) 915–919.
[24] X. Han, S. Shen, Q. Fan, G. Chen, E. Archibong, G. Dotti, Z. Liu, Z. Gu, C. Wang, Red blood cell-derived nanoerythrosome for antigen delivery with enhanced cancer immunotherapy, Sci. Adv. 5 (2019) 1–10, https://doi.org/10.1126/sciadv.aaw6870.
[25] Y.C. Kuo, H.C. Wu, D. Hoang, W.E. Bentley, W.D. D'Souza, S.R. Raghavan, Colloidal properties of nanoerythrosomes derived from bovine red blood cells, Langmuir 32 (2016) 171–179, https://doi.org/10.1021/acs.langmuir.5b03014.
[26] R. Deák, J. Mihály, I. Cs, A. Wacha, G. Lelkes, A. Bóta, Colloids and Surfaces B : Biointerfaces Physicochemical characterization of artificial nanoerythrosomes derived from erythrocyte ghost membranes, 135 (2015) 225–234.
[27] R. Pouliot, A. Saint-Laurent, C. Chypre, R. Audet, I. Vitté-Mony, R.C. Gaudreault, M. Auger, Spectroscopic characterization of nanoErythrosomes in the absence and presence of conjugated polyethyleneglycols: An FTIR and 31P-NMR study, Biochim. Biophys. Acta – Biomembr. 1564 (2002) 317–324, https://doi.org/10.1016/S0005-2736(02)00465-0.
[28] R. Deák, J. Mihály, I.C. Szigyártó, T. Beke-Somfai, L. Turiák, L. Drahos, A. Wacha, A. Bóta, Z. Varga, Nanoerythrosomes tailoring: Lipid induced protein scaffolding in ghost membrane derived vesicles, Mater. Sci. Eng. C. 109 (2020) 110428, https://doi.org/10.1016/j.msec.2019.110428.
[29] W. Tang, M.L. Becker, "Click" reactions: a versatile toolbox for the synthesis of peptide-conjugates, Chem. Soc. Rev. 43 (2014) 7013–7039, https://doi.org/10.1039/c4cs00139g.
[30] S. Chandrudu, P. Simerska, I. Toth, Chemical methods for peptide and protein production, Molecules 18 (2013) 4373–4388, https://doi.org/10.3390/molecules18044373.
[31] V. Hong, N.F. Steinmetz, M. Manchester, M.G. Finn, Labeling live cells by copper-catalyzed alkyne–azide click chemistry, Bioconj. Chem. 21 (2010) 1912–1916, https://doi.org/10.1021/bc100272z.
[32] J.M. Baskin, J.A. Prescher, S.T. Laughlin, N.J. Agard, P.V. Chang, I.A. Miller, A. Lo, J.A. Codelli, C.R. Bertozzi, Copper-free click chemistry for dynamic in vivo imaging, Proc. Natl. Acad. Sci. U. S. A. 104 (2007) 16793–16797, https://doi.org/10.1073/pnas.0707090104.
[33] J.C. Jewett, C.R. Bertozzi, Cu-free click cycloaddition reactions in chemical biology, Chem. Soc. Rev. 39 (2010) 1272, https://doi.org/10.1039/b901970g.
[34] Y. Takayama, K. Kusamori, M. Nishikawa, Click chemistry as a tool for cell engineering and drug delivery, Molecules 24 (2019) 172, https://doi.org/10.3390/molecules24010172.
[35] S. Keereweer, J.D.F. Kerrebijn, P.B.A.A. van Driel, B. Xie, E.L. Kaijzel, T.J.A. Snoeks, I. Que, M. Hutteman, J.R. van der Vorst, J.S.D. Mieog, A.L. Vahrmeijer, C. J.H. van de Velde, R.J. Baatenburg de Jong, C.W.G.M. Löwik, Optical image-guided surgery—where do we stand?, Mol. Imaging Biol. 13 (2) (2011) 199–207, https://doi.org/10.1007/s11307-010-0373-2.
[36] C. Wang, Z. Wang, T. Zhao, Y. Li, G. Huang, B.D. Sumer, J. Gao, Optical molecular imaging for tumor detection and image-guided surgery, Biomaterials 157 (2018) 62–75, https://doi.org/10.1016/j.biomaterials.2017.12.002.
[37] A.M. De Grand, J.V. Frangioni, An operational near-infrared fluorescence imaging system prototype for large animal surgery, Technol Cancer Res. Treat. 2 (2003) 553–562, https://doi.org/10.1177/153303460300200607.
[38] H.S. Peng, D.T. Chiu, Soft fluorescent nanomaterials for biological and biomedical imaging, Chem. Soc. Rev. 44 (2015) 4699–4722, https://doi.org/10.1039/c4cs00294f.
[39] E.A. Owens, M. Henary, G. El Fakhri, H.S. Choi, Tissue-specific near-infrared fluorescence imaging, Acc. Chem. Res. 49 (2016) 1731–1740, https://doi.org/10.1021/acs.accounts.6b00239.
[40] N. Gupta, B. Patel, K. Nahar, F. Ahsan, Cell permeable peptide conjugated nanoerythrosomes of fasudil prolong pulmonary arterial vasodilation in PAH rats, Eur. J. Pharm. Biopharm. 88 (3) (2014) 1046–1055, https://doi.org/10.1016/j.ejpb.2014.10.012.
[41] J. Agnihotri, S. Saraf, S. Singh, P. Bigoniya, Development and evaluation of anti-malarial bio-conjugates: artesunate-loaded nanoerythrosomes, Drug Deliv. Transl. Res. 5 (2015) 489–497, https://doi.org/10.1007/s13346-015-0246-y.
[42] J. Janiak, S. Bayati, L. Galantini, N.V. Pavel, K. Schillén, Nanoparticles with a bicontinuous cubic internal structure formed by cationic and non-ionic surfactants and an anionic polyelectrolyte, Langmuir 28 (48) (2012) 16536–16546, https://doi.org/10.1021/la303938k.
[43] N. Gupta, B. Patel, F. Ahsan, Nano-engineered erythrocyte ghosts as inhalational carriers for delivery of fasudil: preparation and characterization, Pharm. Res. 31 (6) (2014) 1553–1565, https://doi.org/10.1007/s11095-013-1261-7.
[44] J. Yan, J. Yu, C. Wang, Z. Gu, Red blood cells for drug delivery, Small Methods 1 (2017) 1700270, https://doi.org/10.1002/smtd.201700270.